System Sr−Pb−O: Phase Equilibria and Thermodynamics Using Solid-State Cells with Buffer Electrodes

K. T. Jacob* and K. P. Jayadevan

Materials Research Center and Department of Metallurgy, Indian Institute of Science, Bangalore 560 012, India

Received November 11, 1999. Revised Manuscript Received February 29, 2000

The isothermal section of the phase diagram for the system Sr−Pb−O at 1100 K is established by equilibrating 18 compositions in the ternary and analyzing quenched samples using optical and scanning electron microscopy, EDX and XRD. Two ternary oxides, Sr_2PbO_4 and $SrPbO_3$, containing lead in the tetravalent state, are found to be stable. They coexist with PbO. Alloys and intermetallics are in equilibrium with SrO. The high-temperature thermodynamic properties of the ternary oxides are measured for the first time with a novel apparatus. Yttria-stabilized zirconia is used as the solid electrolyte and pure diatomic oxygen gas as the reference electrode. The new feature is the buffer electrode, which is introduced between the reference and measuring electrodes to absorb the electrochemical flux of oxygen through the solid electrolyte. This prevents the polarization of the measuring electrode and ensures accurate data. Measurements are made in the temperature range 860−1090 K. The standard Gibbs energies of formation of Sr_2PbO_4 and $SrPbO_3$ from SrO, PbO, and O_2 are obtained directly from the reversible cell emfs. The results can be represented by the equations: Sr_2PbO_4, $\Delta G^\circ_{f(ox)}$/ J mol^{-1} = −168 650 + 97.87 T/K (±330), and $SrPbO_3$, $\Delta G^\circ_{f(ox)}$/J mol^{-1} = −141 925 + 94.30 T/K (±290).

Introduction

As a part of systematic studies on phase relations and thermodynamic properties of systems of interest in the area of high T_c oxide superconductors, measurements have been made on the ternary system Sr−Pb−O. In the processing of superconducting phases belonging to the system Bi(Pb)−Sr−Ca−Cu−O, Ca_2PbO_4 is formed in the early stages of the reaction.[1] The solid solution $(Ca_{1-x}Sr_x)_2PbO_4$ forms subsequently.[2] Phase diagram studies on the system CaO−SrO−PbO in the temperature range 973−1123 K have been reported.[3,4] However, there is no information on phase relations in the system SrO−PbO(PbO_2) as a function of temperature. Two compounds Sr_2PbO_4 and $SrPbO_3$ and their crystal structures have been reported.[5,6] Lead is present in the tetravalent state in both the compounds. The enthalpy of formation of Sr_2PbO_4 has been measured at 298 K by Idemoto et al.[7] using solution calorimetry. A twin heat conduction type calorimeter was used, with 1.53 M solution of $HClO_4$ as the solvent. The reported enthalpy of formation from elements is −1584.3(±3.5) kJ/mol for a nonstoichiometric sample, composition of which can be represented as $Sr_{1.99}Pb_{1.01}O_{3.99}$. Entropies and Gibbs energies of formation of ternary oxides in the system Sr−Pb−O have not been determined. The purpose of this study was to measure phase relations in the ternary system Sr−Pb−O and Gibbs energies of formation of the stable interoxide compounds. Solid-state cells, which have been extensively used for accurate thermodynamic measurements on oxides,[8] were selected as tools. For design of the measuring electrodes of solid-state cells, prior information on phase relations is required. A new construction of the solid-state cell, with a buffer electrode to absorb the electrochemical flux of oxygen through the solid electrolyte, was used to enhance the accuracy of measurement.

Experimental Section

Materials. Starting materials used in this study had the following nominal purity specifications: Pb, PbO, and $SrCO_3$ were 99.99% pure; and Sr was 99.9% pure. SrO was prepared by thermal decomposition of $SrCO_3$ in a vacuum at 1073 K. The compound Sr_2PbO_4 was made by pelletizing an intimate mixture of SrO and PbO and heating at 1223 K for a total duration of 40 h in air. The pellet was crushed and repelletized twice during this period. The compound $SrPbO_3$ was made by heating an equimolar mixture of SrO and PbO in air at 1103 K for 20 h. The oxide Pb_3O_4 was prepared by oxidizing PbO in oxygen at 800 K. The alloys and intermetallic compounds were prepared by heating the pure metals in the required molar ratios in sealed iron crucibles under flowing inert gas. The identification of interoxide compounds and intermetallic phases was made by powder X-ray diffraction (XRD). High purity

* Person for correspondence.

(1) Braileanu, A.; Zaharescu, M.; Crisan, D.; Segal, E. *Thermochim Acta,* **1995**, *269/270*, 553.
(2) Zaharescu, M.; Braileanu, A.; Crisan, D. *J. Therm. Anal.* **1993**, *40*, 321.
(3) Kitaguchi, H.; Jun, T.; Oda, K.; Miura, Y. *J. Mater. Res.* **1990**, *5*, 1397.
(4) Wong-Ng, W.; Jiang, F.; Cook, L. P. *Physica C* **1996**, *272*, 87.
(5) Tromel, M. *Z. Anorg. Allgem. Chem.* **1969**, *371*, 237.
(6) Shannon, R. D. *J. Solid State Chem.* **1971**, *3*, 184.
(7) Idemoto, Y.; Shizuka, K.; Fueki, K. *Physica C* **1994**, *255*, 127.
(8) Pratt, J. N. *Metall. Trans. A* **1990**, *21*, 1223.

10.1021/cm990728i CCC: $19.00
Published on Web 05/04/2000

(99.999%) gases, O_2, Ar, and their mixtures, were dried by passage through columns containing silica gel and anhydrous $MgClO_4$. Gas mixtures were made by admitting component gases into a cylinder under controlled pressure. The Ar gas, used to provide an inert atmosphere over sealed iron crucibles containing alloys, was deoxidized by passing through columns of copper wool at 723 K and titanium granules at 1173 K. There was negligible change in the mass of the iron crucibles during alloy preparation. Yttria-stabilized zirconia tubes, containing ~8 mol % Y_2O_3, were obtained from Corning Glass.

Phase Relations in the System Sr−Pb−O. Phase relations at 1100 K were explored by equilibrating different mixtures of alloys and compounds for ~100 h, followed by quenching in chilled Hg, and phase identification using optical and scanning electron microscopy, energy dispersive analysis of X-rays (EDX) and XRD. Dense pellets of pure SrO_2 and PbO_2 were used as standards for EDX. Preliminary experiments indicated that ~60 h were sufficient to attain equilibrium. Further heat treatment did not change the composition of the samples. Mixtures containing a metallic phase were equilibrated in sealed iron containers kept under prepurified inert gas flowing at a rate of ~5 mL/s. High purity Ar gas used was dehydrated by passing through anhydrous $MgClO_4$ and P_2O_5, and deoxidized by passing through Cu turnings at 750 K and Ti granules at 1150 K. Samples containing oxide mixtures were equilibrated either in pure oxygen (0.1 MPa) or in evacuated quartz ampules. These samples were contained in stabilized-zirconia crucibles. Zirconia crucibles were closed with a lid before sealing in quartz ampules. To check for the attainment of equilibrium, samples of the same overall composition were prepared using different starting materials. Approach to equilibrium was thus verified from different directions.

To study the nature of decomposition or melting of Sr_2PbO_4 and $SrPbO_3$, the compounds were equilibrated in air at different temperatures for periods up to 20 h. The quenched samples were examined by XRD and EDX.

Emf Measurements using a Solid-State Cell with Three Electrodes. The cell design used for high-temperature emf measurements is shown in Figure 1. It consisted of three distinct compartments, separated by two impervious yttria-stabilized zirconia tubes, each closed at one end. The cell can be represented schematically as follows:

Measuring Electrode O_2 (P'_{O_2}), Pt	$(Y_2O_3)ZrO_2$ No flux	Buffer Electrode O_2(P''_{O_2}), Pt $P''_{O_2} \approx P'_{O_2}$	$(Y_2O_3)ZrO_2$ $\leftarrow$ O^{2-}	Reference Electrode O_2(0.1 MPa), Pt

The measuring and reference electrodes were contained inside separate zirconia tubes. When the difference in the chemical potential of oxygen between these electrodes is substantial, there is always a small flux of oxygen through the zirconia electrolyte separating them, even in the absence of physical porosity.[9] The electrochemical permeability is caused by the coupled transport of oxygen ions and holes (or electrons) in the solid electrolyte under the oxygen potential gradient. This flow of oxygen can be stopped only by opposing it with an external dc voltage exactly equivalent to the oxygen chemical potential difference.[10]

An electrochemical flux of oxygen would cause polarization of multiphase solid electrodes. The chemical potential of oxygen in the microsystem near the solid electrode/electrolyte interface would be altered because of the semipermeability of the electrolyte to oxygen. The buffer electrode, introduced between reference and measuring electrodes was designed to act as a sink for the oxygen flux and prevent the flux from reaching the measuring electrode. The buffer electrode was maintained at an oxygen chemical potential close to that of the measuring electrode. Since there was no significant difference between the chemical potentials of the buffer and measuring electrodes, a driving force for transport of oxygen through the zirconia tube separating these electrodes did not exist. The measuring electrode therefore remained unpolarized. Pure oxygen gas at a pressure of 0.1 MPa flowing over a platinized surface of zirconia constituted the primary reference standard for oxygen potential and formed an unpolarizable electrode. Thus, the three-electrode design of the cell prevented error in emf caused by polarization of the measuring electrode. Measuring the emf between the buffer and measuring electrodes assessed the magnitude of the polarization effect.

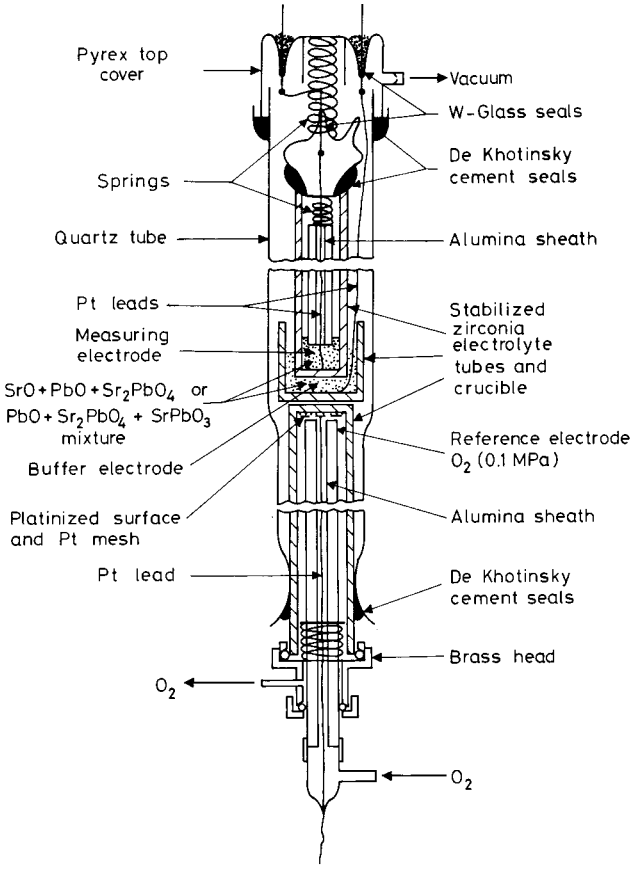

Figure 1. Schematic diagram of the new apparatus for emf measurements on Sr_2PbO_4 and $SrPbO_3$ with a buffer electrode interspaced between measuring and reference electrodes.

Construction of the high temperature galvanic cell was rendered more difficult by the introduction of the buffer electrode. Moreover, in one of the cells used in this study, the partial pressure of oxygen at the measuring electrode was quite appreciable, especially at the higher temperatures. Therefore, the static sealed design used by Charette and Flengas[11] was found to be more appropriate than other designs that employ either dynamic vacuum or inert gas flow over the electrodes.[8,12]

The measuring electrode consisted of an intimate mixture of SrO, PbO, and Sr_2PbO_4 in the molar ratio of 1:1:1.5 in cell I, and a mixture of PbO, Sr_2PbO_4, and $SrPbO_3$ in the ratio 1:1:1.5 in cell II. Excess of Sr_2PbO_4 and $SrPbO_3$ were taken, since these phases had to decompose initially to establish oxygen pressure in the apparatus. The three-phase mixture was rammed against the closed end of a stabilized zirconia tube with a Pt lead embedded in the mixture. An alumina sheath was used to insulate this lead and to press the measuring electrode against the flat end of the zirconia tube. The top of the zirconia tube was closed with a tight-fitting bell-shaped

(9) Fouletier, J.; Fabry, P.; Kleitz, M. *J. Electrochem. Soc.* **1976**, *123*, 204.

(10) Jacob, K. T.; Jeffes, J. H. E. *Trans. Inst. Min. Metall., Sect. C* **1971**, *80*, C181.

(11) Charette, G. G.; Flengas, S. N. *J. Electrochem. Soc.* **1968**, *115*, 796.

(12) Kale, G. M.; Jacob, K. T. *Metall. Trans. B* **1992**, *23*, 57.

Pyrex tube, which supported a tungsten electrode connection sealed into the glass. The joint between the bell and the zirconia tube was sealed with De Khotinsky cement. A metal spring placed between the bell and the alumina sheath applied pressure on the measuring electrode. The assembled measuring electrode half-cell was first evacuated using a sidearm tube shown in the diagram, heated to ~400 K, and then the tube was flame-sealed under vacuum.

The measuring half-cell assembly rested on a buffer electrode contained in a stabilized-zirconia crucible. The buffer had the same phase composition as the measuring electrode initially. Thus, the partial pressure of oxygen in the buffer was the same as that of the measuring electrode at the start of the experiment. However, in the course of the experiment, the oxygen partial pressure in the buffer increased to a value equivalent to ~6 mV higher than that of the measuring electrode, because of the oxygen flux from the reference side. The buffer electrode was prepared by consolidating an intimate mixture of constituent phases in the zirconia crucible, with a Pt lead embedded in the powder. To minimize vaporization of PbO from the buffer electrode, it was covered with a thick layer of zirconia powder. The vapor pressure of PbO over the electrode is not very significant in the temperature range of measurement.

The zirconia crucible containing the buffer electrode rested on another inverted zirconia tube. The mating surfaces of the crucible and tube were polished with diamond paste to minimize resistance. The inside surface of the inverted zirconia tube was platinized. A platinum gauze was pressed against the closed end of the inverted tube, using an alumina sheath. A Pt lead, spot-welded to the gauze, passed through the alumina sheath. The open end of the inverted zirconia tube was fitted with a brass head. Pure oxygen gas at a pressure of 0.1 MPa was flowed through the inverted zirconia tube at a rate of 3 mL/s. A cascade of bubblers placed at the gas exit controlled the pressure inside the tube. The oxygen electrode served as the reference.

The cell was assembled inside a fused quartz enclosure. The inverted zirconia tube containing the reference electrode was first fixed inside the vertical quartz enclosure with De Khotinsky cement. The zirconia crucible containing the buffer electrode was placed on top of the inverted tube. The measuring electrode assembly was then loaded into the crucible. The annular space between the zirconia tube and crucible was filled with the buffer electrode mixture. The measuring electrode assembly was pressed down by means of a second metal spring placed between the bell and the top Pyrex cover. The top cover supported two tungsten glass seals through which electrical connections were made. All electrode connections were silver soldered. Finally, the top cover was cemented in place by melting the De Khotinsky cement in the ring container shown in the diagram. The cement was allowed to solidify while pressing the top cover against the spring. Then the outer quartz enclosure was also evacuated from a sidearm tube and flame-sealed under vacuum. The top half of the cell assembly, shown in Figure 1, was identical to that developed by Charette and Flengas.[11]

The entire assembly shown in Figure 1 was placed inside a vertical resistance furnace, with the electrodes located in the even-temperature zone (±1 K). The upper and lower parts of the assembly, where cement seals were located, remained at room temperature during measurements. A Faraday cage made from stainless steel foil was placed between the furnace and the cell assembly. The foil was grounded to minimize induced emf on cell leads. The temperature of the furnace was controlled to ±1 K. The temperature was measured by a Pt/Pt−13% Rh thermocouple, calibrated against the melting point of gold and placed adjacent to the zirconia crucible in the even-temperature zone of the furnace. The cell potentials were measured with a high-impedance digital voltmeter with a sensitivity of ±0.01 mV. The potential readings were corrected for small thermal emfs, measured separately.

Although the cell assembly shown in Figure 1 consists of three electrode compartments, the cell potential is determined only by the chemical potentials of oxygen in the measuring and reference electrodes. Thus, the effective cells used in this study can be concisely written as

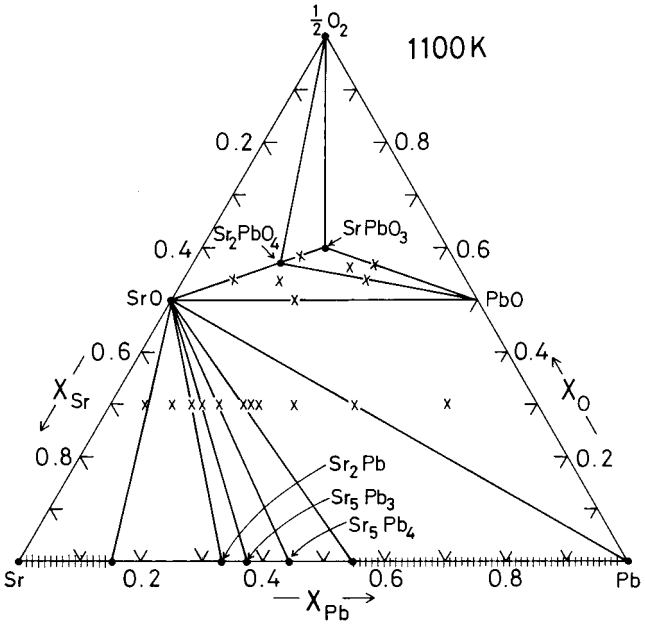

Figure 2. Isothermal section of the phase diagram for the system Sr−Pb−O at 1100 K. The average composition of samples examined in this study is shown by X.

$$\text{Pt, SrO + PbO + } Sr_2PbO_4 \text{||}(Y_2O_3)\ ZrO_2\text{||}O_2\ (0.1\ \text{MPa}),\ \text{Pt} \quad \text{(I)}$$

$$\text{Pt, PbO + } Sr_2PbO_4 + SrPbO_3\text{||}(Y_2O_3)\ ZrO_2\text{||}O_2\ (0.1\ \text{MPa}),\ \text{Pt} \quad \text{(II)}$$

The cells are written such that the right-hand electrodes are positive.

Results and Discussion

Phase Diagram. The isothermal section of equilibrium phase diagram for the system Sr−Pb−O at 1100 K, composed from the results obtained by isothermal equilibration and phase identification of quenched samples by optical and scanning electron microscopy, EDX and XRD, is shown in Figure 2. The average composition of the samples studied is shown by cross marks. Identical phase relations were obtained despite different starting materials used for making samples at the specified compositions. Only one oxide, PbO, was found along the binary Pb−O. PbO can be oxidized in air to Pb_3O_4 at lower temperatures. Along the binary Sr−O, SrO is the only stable phase at 1100 K. Liquid alloys form along two regions on the binary Sr−Pb: $0 \le X_{Pb} \le 0.153$ and $0.546 \le X_{Pb} \le 1.0$. Three intermetallic compounds, Sr_2Pb, Sr_5Pb_3 and Sr_5Pb_4, were found to be stable. All alloys and intermetallic compounds are in equilibrium with SrO.

Two ternary oxides, Sr_2PbO_4 and $SrPbO_3$ were detected in the system. The compounds were formed only when mixtures of SrO and PbO in the appropriate ratio were heated in pure O_2 or air. The component binary oxides were found not to react when the mixture was heated in evacuated quartz ampules. The compounds contain Pb in tetravalent state. The compound, Sr_2PbO_4, has an orthorhombic lattice with space group *Pbam* and lattice parameters $a = 0.6162$, $b = 1.008$, and $c = 0.3502$

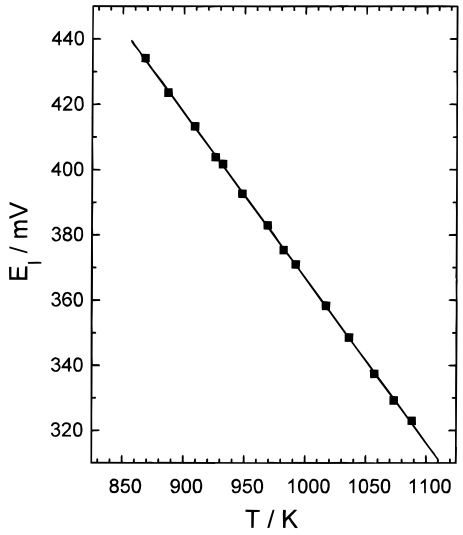

Figure 3. Emf of cell I, with SrO + PbO + Sr_2PbO_4 as the working electrode, as a function of temperature.

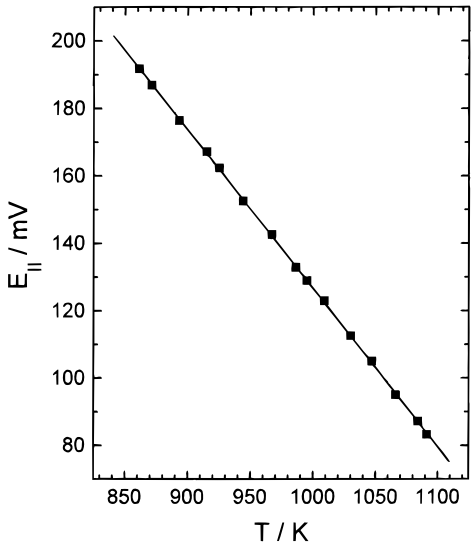

Figure 4. Temperature dependence of the emf of cell II having PbO + Sr_2PbO_4 + $SrPbO_3$ as the working electrode.

nm. It contains chains of PbO_6 octahedra similar to those of Pb_3O_4. Although this compound has the same space group as Pb_3O_4 below 240 K, there are large differences in lattice parameters. The cell parameters for Pb_3O_4 at 200 K are $a = 0.8818$, $b = 0.8803$, and $c = 0.6562$ nm.[13] At room temperature the space group of Pb_3O_4 is $P4_2/mbc$, with $a = 0.8813$ and $c = 0.6565$ nm. Therefore, significant solid solubility between Pb_3O_4 and Sr_2PbO_4 is unlikely. The phases that coexist with Sr_2PbO_4 at 1100 K are PbO (yellow), SrO, $SrPbO_3$, and O_2 gas (0.1 MPa). The compound $SrPbO_3$ has an orthorhombic unit cell (space group $Pbnm$) with $a = 0.5860$, $b = 0.5957$, and $c = 0.8325$ nm. The compound coexists with Sr_2PbO_4, PbO, and O_2 at 1100 K. Liquid phase was not observed along the join SrO−PbO in pure oxygen at 1100 K. The phase diagram suggests that the Gibbs energy of formation of Sr_2PbO_4 from SrO and PbO and O_2 can be obtained by measuring the oxygen partial pressure in the three-phase region SrO + PbO + Sr_2PbO_4. Measurement of the oxygen chemical potential corresponding to the three-phase field, PbO + Sr_2PbO_4 + $SrPbO_3$, can be used for evaluating thermodynamic properties of $SrPbO_3$.

Microscopic and XRD examination of Sr_2PbO_4 samples quenched from different temperatures indicated that it decomposes in air at 1361(±7) K to solid SrO and liquid melt (SrO−PbO−PbO_2), with $\eta_{Pb}/(\eta_{Sr} + \eta_{Pb}) = 0.50(\pm 0.04)$. Similarly, $SrPbO_3$ was found to decompose to Sr_2PbO_4 and liquid (SrO−PbO−PbO_2) characterized by $\eta_{Pb}/(\eta_{Sr} + \eta_{Pb}) = 0.77(\pm 0.04)$ at 1152(±5) K in air.

Gibbs Energies of Formation of Sr_2PbO_4 and $SrPbO_3$. The reversible emfs of cells I and II are shown as a function of temperature in Figures 3 and 4, respectively. The reversibility of the emfs was established by microcoulometric titration in both directions. A small current (∼50 μA) was passed through the cell, using an external potential source for ∼5 min and the open-circuit emf was subsequently monitored as a function of time. The emf was found to return to the steady value before each titration. During each titration, the chemical potential of oxygen at each electrode was displaced from equilibrium by an essentially infinitesimal amount. Since the electrodes returned to the same potential after such displacements in opposite directions, equilibrium was presumed to be attained. The emf was not affected by the flow rate of oxygen through the reference electrode in the range 2−5 mL/s. The emf was also found to be reproducible on temperature cycling in the range 860−1090 K.

With the three-electrode design of the cell, the emfs were steady (±0.7 mV) for periods in excess of 10 h. The emf of the buffer electrode measured against the reference was almost identical to that of the measuring electrode at the beginning of the experiments. As a consequence of the flux of oxygen from the reference electrode, the emf of the buffer electrode against the reference gradually decreased to a value ∼6 mV lower than that of the measuring electrode by the end of the experiment with cell I. This clearly demonstrated the need for the buffer to absorb the oxygen flux and protect the measuring electrode from being disturbed. Polarization of the three-phase electrode was less significant with cell II: the emf of the buffer electrode against the reference was only 2 mV lower than that of the measuring electrode. The reduced polarization with cell II may be the result of smaller driving force for oxygen transport through the solid electrolyte. The emfs of cells I and II are linear functions of temperature, as seen from Figures 3 and 4. The least-squares regression analysis of the emfs gives

$$E_I/\text{mV} = 873.9 - 0.5071\ T/\text{K}\ (\pm 1.7) \qquad (1)$$

$$E_{II}/\text{mV} = 596.9 - 0.4702\ T/\text{K}\ (\pm 1.2) \qquad (2)$$

The uncertainty estimates are based on random (2σ) and systematic errors in measurement of emf and temperature. The systematic errors include uncertainties in the calibration of the thermocouple and high-impedance digital voltmeter. The oxygen potential corresponding to the three-phase equilibrium between SrO, PbO and Sr_2PbO_4, and the Gibbs energy of formation of Sr_2PbO_4 from component oxides (SrO, PbO) and oxygen, defined by the equation:

(13) Garnier, P.; Calvarin, G.; Weigel, D. *J. Solid State Chem.* **1976**, *16*, 55.

$$2SrO + PbO + {}^1/_2O_2 \rightarrow Sr_2PbO_4 \quad (3)$$

can be obtained directly from the emf of cell I. Since pure SrO, PbO, and Sr_2PbO_4 at unit activities are present at the measuring electrode, the standard Gibbs energy change for reaction 3 is related to the relative oxygen chemical potential at the electrode. As pure oxygen at 0.1 MPa is used as the reference electrode, the emf of cell I is directly related to the standard Gibbs energy change for reaction 3:

$$\Delta G^\circ_{r(3)}/\text{J mol}^{-1} = 0.5\ \Delta\mu_{O_2}/\text{J mol}^{-1} = -2FE_I$$
$$= -168\ 650 + 97.87\ T/\text{K}\ (\pm 330) \quad (4)$$

where F is the Faraday constant. The yellow (massicot, β) form is the reference state for PbO. At 1100 K, the normalized oxygen partial pressure (P_{O_2}/P°) corresponding to the three-phase equilibrium is 1.61×10^{-6}, where P° represents the standard pressure. The temperature-independent term on the right-hand side of eq 4 represents the "second law" enthalpy change for reaction 3 at a mean experimental temperature of 980 K, and has a value of −168.7 (±2.0) kJ/mol. Since heat capacity of Sr_2PbO_4 has not been measured as a function of temperature, the enthalpy change for reaction 3 at 298.15 K cannot be assessed exactly. However, if the enthalpy change ($\Delta H^\circ_{r(3)}$) is assumed to be independent of temperature, then the standard enthalpy of formation of Sr_2PbO_4 from elements at 298.15 K can be estimated by combining the results obtained in this study with standard enthalpies of formation of SrO and PbO.[14] The estimated value for the standard enthalpy of formation from elements at 298.15 K is −1567.1(±6) kJ/mol. The corresponding value obtained by Idemoto et al.[7] from solution calorimetry is −1584.3 (±3.5) kJ/mol. The composition of the samples used by Idemoto et al.[7] is $Sr_{1.99}Pb_{1.01}O_{3.99}$. Part of the difference in enthalpy of formation obtained in the two studies (17.2 kJ/mol) may be attributed to the change in $\Delta H^\circ_{r(3)}$ with temperature and the nonstoichiometry of the calorimetric sample. It is interesting to note that a difference of 11.8 kJ/mol exists between enthalpy of formation of isostructural Ca_2PbO_4 obtained from high-temperature emf studies[15] and room-temperature calorimetry.[6] It would be useful to measure the low- and high-temperature heat capacities of Sr_2PbO_4 so that a more complete assessment of thermodynamic data for the compound can be performed.

The oxygen potential corresponding to the three-phase equilibrium among PbO, Sr_2PbO_4, and $SrPbO_3$, defined by the reaction:

$$0.5Sr_2PbO_4 + 0.5PbO + 0.25O_2 \rightarrow SrPbO_3 \quad (5)$$

can be directly obtained from the emf of cell II.

$$\Delta G^\circ_{r(5)}/\text{J mol}^{-1} = 0.25\ \Delta\mu_{O_2}/\text{J mol}^{-1} = -FE_{II}$$
$$= -57\ 600 + 45.37\ T/\text{K}\ (\pm 230) \quad (6)$$

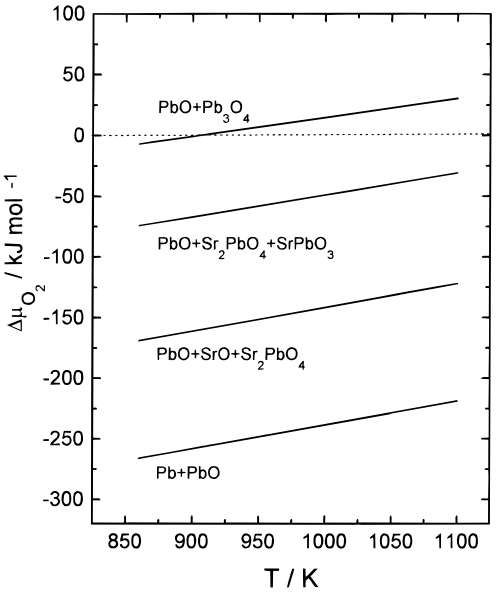

Figure 5. Temperature dependence of oxygen chemical potential for different phase fields in the system Sr−Pb−O.

Combining eqs 3 and 5, the standard Gibbs energy of formation of $SrPbO_3$ from PbO, SrO and O_2 can be derived. For the reaction,

$$SrO + PbO + 0.5O_2 \rightarrow SrPbO_3 \quad (7)$$

$$\Delta G^\circ_{r(7)}/\text{J mol}^{-1} = -141\ 925 + 94.30\ T/\text{K}\ (\pm 230) \quad (8)$$

There are no previous thermodynamic measurements on $SrPbO_3$ for comparison. Accurate values for the standard Gibbs energy of formation of PbO_2 are not available at the experimental temperatures to assess the Gibbs energies of formation of Sr_2PbO_4 from its constituent oxides SrO and PbO_2. PbO_2 is unstable at these temperatures. The temperature dependence of the oxygen chemical potential for various phase fields in the system Sr−Pb−O is shown in Figure 5. It is seen that oxygen potential lines do not cross, indicating that the phase relations are basically unaffected by temperature in the experimental range.

Computation of Phase Diagrams. The oxygen potential diagram for the system Sr−Pb−O at 1100 K, composed from the results of this study and data from the literature[14−17] on binary oxides is shown in Figure 6. The composition variable is metallic fraction, $\eta_{Pb}/(\eta_{Sr} + \eta_{Pb})$, where η_i represents moles of component i. Since oxygen is not included in the composition parameter, information on oxygen nonstoichiometry cannot be displayed on the diagram. Nevertheless, the diagram provides useful information on the oxygen potential range for the stability of various phases. The diagram is complementary to the conventional Gibbs triangle representation of phase relations in ternary systems, where phase composition can be unambiguously displayed. All the topological rules of construction for conventional temperature−composition phase diagrams

(14) Pankratz, L. B. *Thermodynamic Properties of Elements and Oxides*; U.S. Bureau of Mines Bull. 672; U.S. Government Printing Office: Washington, DC, 1982.
(15) Jacob, K. T.; Jayadevan, K. P. *J. Mater. Chem.* **1997**, *7*, 2407.
(16) Jacob, K. T.; Jeffes, J. H. E. *Trans. Inst. Min. Metall., Sect. C* **1971**, *80*, C32.
(17) Knacke, O.; Kubaschewski, O.; Hesselmann, K *Thermochemical Properties of Inorganic Substances*, 2nd ed.; Springer-Verlag: Berlin 1991; Vol. II.

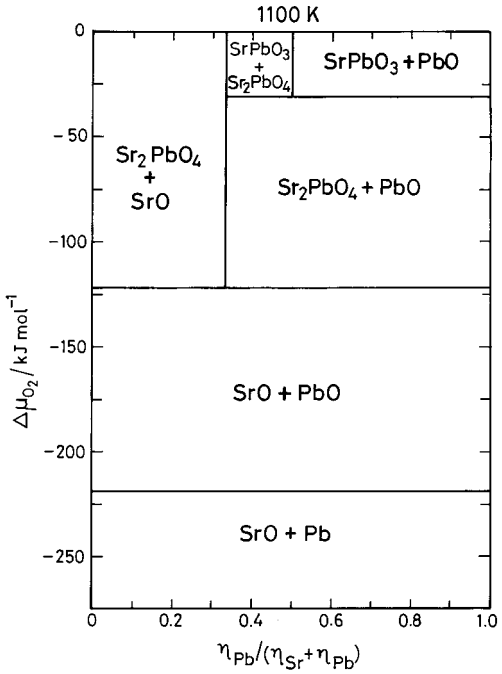

Figure 6. Oxygen chemical potential diagram for the system Sr−Pb−O at 1100 K.

are applicable to the oxygen potential diagram shown in Figure 6.

The standard Gibbs energies of formation of solid PbO and Pb_3O_4 used in the computation are taken from earlier measurements.[14,15] For the reaction,

$$Pb + {}^1/_2O_2 \rightarrow PbO \quad (9)$$

$$\Delta G_f^\circ/\text{J mol}^{-1} = -218\,100 + 98.89\ T/\text{K}\ (\pm 420) \quad (10)$$

$$3PbO + {}^1/_2O_2 \rightarrow Pb_3O_4 \quad (11)$$

$$\Delta G_{r(11)}^\circ/\text{J mol}^{-1} = -70\,060 + 77.5\ T/\text{K}\ (\pm 150) \quad (12)$$

The standard state for PbO is the yellow form.

When three condensed phases and a gas-phase coexist at equilibrium in a ternary system such as Sr−Pb−O, the system is monovariant; at a fixed temperature, three condensed phases coexist only at a unique partial pressure of oxygen. Horizontal lines on the diagram therefore represent three-phase equilibria. The phase equilibria at very low oxygen potentials between alloys and intermetallic compounds on one hand, and SrO on the other, are not shown in Figure 6, since activity data for the metallic phases required for the calculation are not available. The oxygen potentials are too low to be measured by currently available techniques.[8] Similar diagrams at other temperatures can be readily computed from the thermodynamic data.

Phase Diagrams at Constant Oxygen Partial Pressure. Phase relations can also be computed from thermodynamic data as a function of temperature at constant oxygen partial pressures. The computed phase diagrams in air ($P_{O_2} = 2.12 \times 10^4$ Pa) and an oxygen partial pressure of 10.13 Pa are shown in Figure 7. The decomposition temperatures for the oxides $Pb_{12}O_{17}$, $Pb_{12}O_{19}$, PbO_2, and SrO_2 are not accurately known.[18]

Table 1. Estimate of Change in Standard Gibbs Energy for the Decomposition of Higher Oxides of Pb and Sr

reaction	ΔG°/J mol^{-1}
$12PbO_2 \rightarrow Pb_{12}O_{19} + {}^5/_2O_2$	256 950 − 450 T
$Pb_{12}O_{19} \rightarrow Pb_{12}O_{17} + O_2$	117 000 − 180 T
$Pb_{12}O_{17} \rightarrow 4Pb_3O_4 + {}^1/_2O_2$	59 760 − 90 T
$SrO_2 \rightarrow SrO + {}^1/_2O_2$	59 580 − 96.1 T

Several conflicting reports appear in the literature. The following decomposition temperatures in pure oxygen (0.1 MPa) are selected for constructing the schematic diagram: $Pb_{12}O_{17}$ (664 K[19,20]), $Pb_{12}O_{19}$ (650 K[19]), PbO_2 (571 K[19,20]), and SrO_2 (620 K[21]). The estimated standard Gibbs energy changes accompanying their decomposition are summarized in Table 1. The estimates are based on the selected decomposition temperatures and an entropy change of 180 J K^{-1} mol^{-1} of O_2 for decomposition of higher oxides of lead. Heat capacity as a function of temperature has not been measured for $Pb_{12}O_{19}$ and $Pb_{12}O_{17}$ for calculating their entropies. For SrO_2, the entropy change for dissociation is derived from measured heat capacity data.[17]

The Gibbs energy change associated with the melting of PbO (yellow) is computed using an average value of three independent determinations of the enthalpy of fusion:[22−24]

$$PbO\ (s, \text{yellow}) \rightarrow PbO\ (l) \quad (13)$$

$$\Delta G_{r(13)}^\circ/\text{J mol}^{-1} = 26\,700 - 23.04\ T/\text{K}\ (\pm 200) \quad (14)$$

The Gibbs energy change associated with melting of SrO is obtained from the enthalpy measurements of Igrashov et al.[25] using drop calorimetry. The enthalpy of fusion is 80.95 kJ/mol at the melting temperature 2870 (±20) K. The difference in heat capacities of solid and liquid SrO[25] is taken into account in computing the Gibbs energy change for melting of SrO at lower temperatures.

The decomposition temperature of Sr_2PbO_4 and $SrPbO_3$ are considerably higher than that for Pb_3O_4, $Pb_{12}O_{17}$, $Pb_{12}O_{19}$, PbO_2, and SrO_2 at all partial pressures of oxygen. Because of strong binding between the component oxides SrO and PbO_2 in the ternary phases Sr_2PbO_4 and $SrPbO_3$, the activity of PbO_2 in these compounds is substantially lowered. The strong interaction between SrO and PbO_2, and the absence of ternary oxides containing Pb^{2+} ion, is indicative of the stronger acidic character of PbO_2 in comparison with PbO in the presence of group 2 oxides. It would be interesting to see if this is a general effect of group 2 oxides on group 4 oxides. Studies on systems containing oxides of Sn and Ge would be useful for testing the general trend. The strong interaction between SrO and PbO_2 accounts for the high decomposition temperature of Sr_2PbO_4 and

(18) Wriedt, H. A. *Bull. Alloy Phase Diagrams* **1988**, *9*, 106.
(19) Butler, G.; Copp, J. L. *J. Chem. Soc.* **1956**, 725.
(20) Abadir, M. F.; Gadalla, A. M.; El-Agamawi, Y. M. *Trans. J. Br. Ceram. Soc.* **1976**, *75*, 68.
(21) Holtermann, C. B. *Ann. Chim. Paris* **1940**, *14*, 121.
(22) Rodigina, E. N.; Gomel'skii,K. Z.; Luginina,V. F. *Russ. J. Phys. Chem.* **1961**, *35*, 884.
(23) Knake, O.; Prescher, K. *Erzmetall* **1964**, *17*, 28.
(24) Warner, A. E. W.; Roye, M. P.; Jeffes, J. H. E. Private communication.
(25) Igrashov, Kh.; Tarasov, V. D.; Chekhovskii, V. Ya. *Teplofiz. Vys. Temp.* **1985**, *23*, 86.

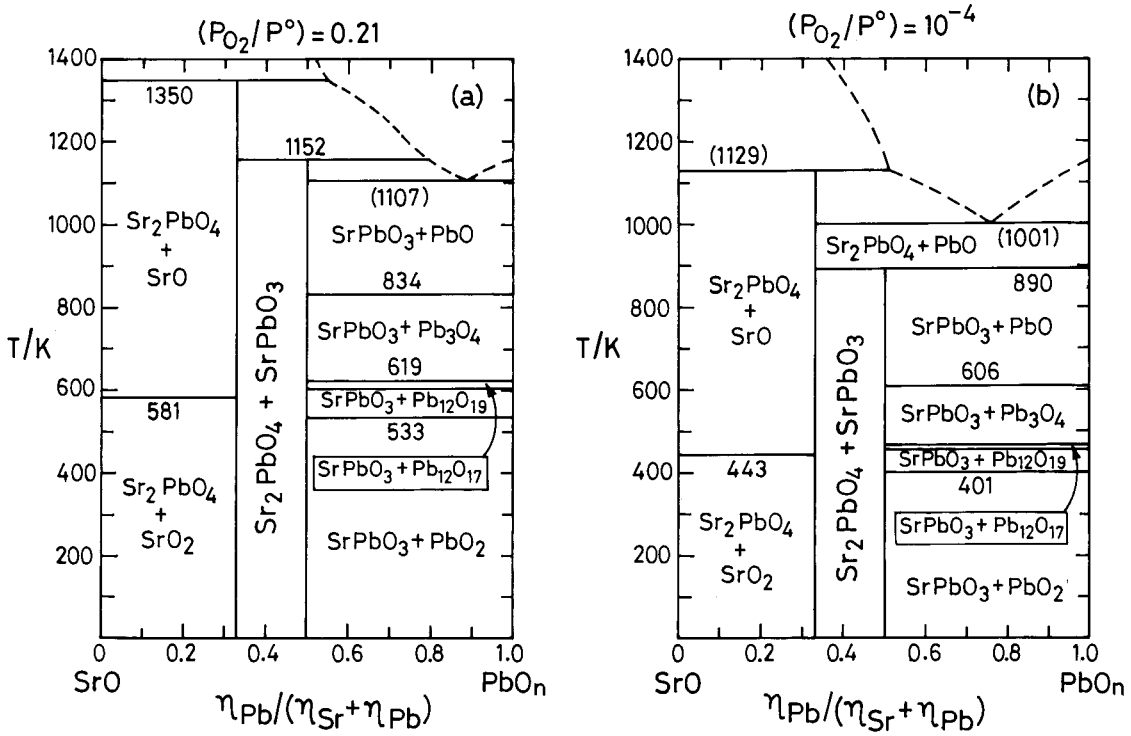

Figure 7. Phase diagram for the system Sr−Pb−O at fixed oxygen partial pressures: (a) air (P_{O_2} = 2.12 × 10^4 Pa) and (b) P_{O_2} = 10.13 Pa (10^{-4} atm).

$SrPbO_3$. Figure 7 shows that the temperature−composition diagram is very sensitive to oxygen partial pressure in the ambient atmosphere. An interesting feature is the effect of oxygen partial pressure on the nature of eutectic reaction near the PbO-rich side. In air, the liquid-phase decomposes to $SrPbO_3$ and PbO (yellow). At an oxygen partial pressure of 10.13 Pa, the liquid decomposes to Sr_2PbO_4 and PbO (yellow).

Since information on oxygen stoichiometry cannot be shown in a two-dimensional representation of ternary phase equilibria at constant oxygen partial pressure, a schematic three-dimensional sketch of subsolidus phase relations in the subsystem SrO−PbO−O is presented in Figure 8. Below the decomposition temperature of Pb_3O_4 (904 K[15]), a new three-phase region (PbO + Pb_3O_4 + $SrPbO_3$) is generated. Below the decomposition temperature of $Pb_{12}O_{17}$, yet another three-phase region (Pb_3O_4 + $Pb_{12}O_{17}$ + $SrPbO_3$) is obtained. A further decrease in temperature gives rise to the appearance of $Pb_{12}O_{19}$, resulting in an additional three-phase field $Pb_{12}O_{17}$ + $Pb_{12}O_{19}$ + $SrPbO_3$. At lower temperatures ($T \leq 620$ K), SrO_2 becomes stable and two additional three-phase regions, SrO + Sr_2PbO_4 + SrO_2 and Sr_2PbO_4 + $SrPbO_3$ + SrO_2 are generated. On further cooling PbO_2 is formed, generating a three-phase field $Pb_{12}O_{19}$ + PbO_2 + $SrPbO_3$. The ternary oxide $SrPbO_3$ can exist in equilibrium with all five oxides of lead, PbO, Pb_3O_4, $Pb_{12}O_{17}$, $Pb_{12}O_{19}$, and PbO_2 below the decomposition temperature of PbO_2, and with SrO_2. It does not coexist with SrO. Each three-phase region is associated with a unique oxygen partial pressure at constant temperature. As one proceeds from a specific composition on the binary SrO−PbO toward the oxygen apex along a path of constant ratio η_{SrO}/η_{PbO} on an isothermal section of the phase diagram, phase fields with increasing oxygen partial pressure are encountered.

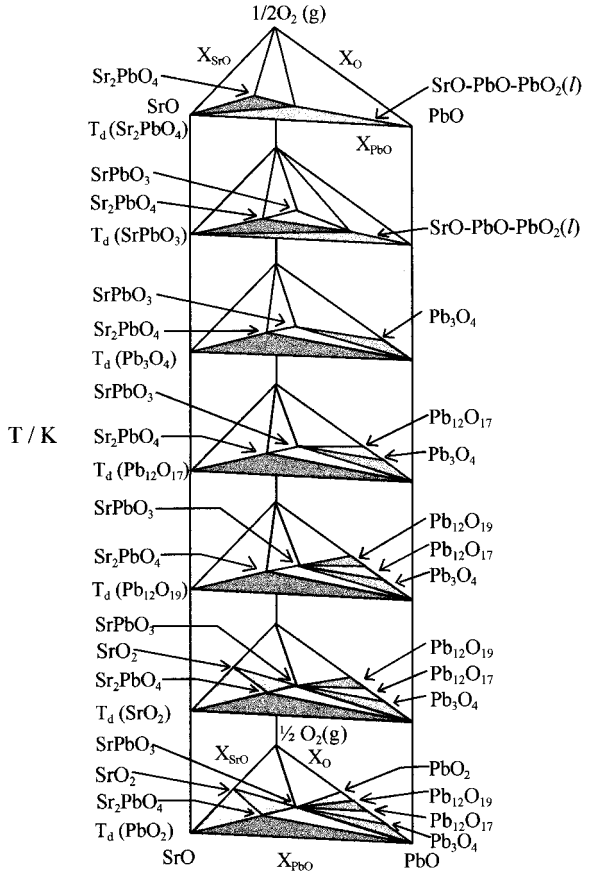

Figure 8. Schematic temperature−composition phase diagram for the ternary system SrO−PbO−O.

Conclusion

An experimentally validated ternary equilibrium phase diagram has been constructed for the system Sr−Pb−O at 1100 K. In this system, there exist two ternary

oxides, Sr_2PbO_4 and $SrPbO_3$. They are stable in oxygen and air, but decompose when oxygen partial pressure is reduced below a critical value. Solid-state cells based on yttria-stabilized zirconia were used to measure the oxygen potential corresponding to three-phase equilibria $PbO + Sr_2PbO_4 + SrO$ and $PbO + Sr_2PbO_4 + SrPbO_3$. There was negligible solid solubility between these oxides. Hence, the standard Gibbs energies of formation of Sr_2PbO_4 and $SrPbO_3$ were derived from the reversible emfs of the cells. An advanced design of the apparatus with a buffer electrode was used to prevent polarization of the three-phase electrode in each cell. Thermodynamic data were used for deriving an oxygen potential diagram for the system Sr−Pb−O at 1100 K, and phase relations as a function of temperature at constant oxygen partial pressures. The data can also be used for computation of phase relations in higher order systems.

Acknowledgment. One of the authors (K.P.J.) wishes to thank the Council of Scientific and Industrial Research (CSIR), India, for a Senior Research Fellowship (SRF).

CM990728I